Progress In Electromagnetics Research M, Vol. 56, 157–167, 2017

Variation in Phase Shift of Phase Arrangements on Magnetic Field underneath Overhead Double-Circuit HVTLs: Field Distribution and Polarization Study

Akinlolu A. Ponnle, Kazeem B. Adedeji*, Bolanle T. Abe, and Adisa A. Jimoh

Abstract—The currents flowing through a transmission line produce a rotating magnetic field of vertical and horizontal components which are orthogonal in space and vary with time. Buried and aerial metallic pipelines that run parallel to or are placed in the vicinity of overhead AC high voltage transmission lines are affected by this field resulting in an induced voltage on the pipelines. Several related studies and safety standards dealing with this problem have been published. Nevertheless on a multi-circuit line, the issue of current phase shift variation has not been fully covered yet. This paper provides a detailed analysis of the effect of current phase shifts on the magnetic field distribution and polarization pattern around power lines using analytical approach from electromagnetic field theory. In this study, not only the variation of the filed distribution with phase arrangements and phase shifts is further established, but also the characteristic nature of the variation of the field distributions for six phase arrangements is examined in more detail. The results show that the magnetic field distribution at the ground level and the spatial distribution of the magnetic field polarization ratio vary significantly with the phase sequence arrangement as well as the current phase shifts between the two circuits. The field polarization differs at different locations. The information from the results can be useful for consideration in designing an effective AC mitigation technique and in placing pipelines in the utility corridor with power lines. Pipelines should be placed in a region of minimum field intensity within the right-of-way of the line, in order to have minimal induction on the pipeline in normal operating conditions of the line.

1. INTRODUCTION

The currents carried by high voltage power transmission line (HVTL) conductors create a time varying magnetic field around the conductors of the power lines. This magnetic field is made up of vertical and horizontal components which are orthogonal in space and vary with time thereby giving rise to a rotating field which traces an ellipse in a plane perpendicular to the axis of the conductors. Several research efforts have been conducted in the past and in recent time to assess the health effect of the magnetic field on human beings [1, 2] as well as its effect on metallic pipelines [3–8]. Aerial and underground metallic pipelines that are placed in the same right-of-way with high voltage power lines are affected by inductive coupling due to this field, under both nominal operating conditions and short circuit conditions on the power line [3, 5, 6]. Because of the continuous growth in energy consumption, there are more tendencies to site pipelines and power lines along the same routes, and the number of situations is on the increase where new pipelines have to be installed next to existing power lines. The induced voltage on the pipelines is known to enhance accelerated corrosion of the pipeline material, even though till today, the

Received 3 November 2016, Accepted 19 January 2017, Scheduled 5 May 2017
* Corresponding author: Kazeem B. Adedeji (adedejikb@tut.ac.za).
The authors are with the Department of Electrical Engineering, Faculty of Engineering and the Built Environment, Tshwane University of Technology, Pretoria, South Africa.

exact mechanism by which it occurs is not yet fully understood in the literature. This is usually referred to as AC corrosion by AC interference. The AC corrosion is due to an exchange of AC-induced current and voltage between the pipeline and the surrounding soil. It poses a danger to working personnel on the pipelines and also affects the performance of cathodic protection of the pipelines [9–11].

The magnitude of the induced voltage varies with the planar magnetic field distribution below the HVTL in which the pipeline is located, which also varies with some parameters of the HVTL. For buried metallic pipelines that run along the power line, the horizontal component of the magnetic field, if the ground is assumed to be non-magnetic and of finite conductivity, plays a major role in the induction [12]. Since most buried pipelines are usually located not far from the ground surface, the distribution of the magnetic field horizontal component at the ground level cannot be overlooked. Many works have studied the effect of different parameters on the produced magnetic field from overhead HVTLs and twisted cables either by computations or measurement, some of which can be found in [13–17]. One of the ways to mitigate the effect of the AC interference is to reduce the strength of the magnetic fields underneath the power lines. Moreover, the magnetic field vector which varies and changes both in space and time can be represented as a rotating vector which traces an ellipse in a plane perpendicular to the conductors [14]. The orientation of the field vector and the shape of the ellipse determines the polarization.

On double-circuits power lines, there are six possible phase configurations of the second circuit with respect to the first circuit. Assuming the phase conductors are labelled A, B, and C, the phase arrangement of the first circuit to be ABC, and the combinations with the second circuit are ABC-ABC, ABC-CBA, ABC-BAC, ABC-CAB, ABC-ACB and ABC-BCA. With three or more circuits on power lines, the number of possible combinations to simulate increases. The phase shifts between corresponding phase currents in double-circuit lines can also affect the magnetic field distribution significantly. Displacement between corresponding phase currents in a double-circuit line can occur if the two single-circuit lines making up the double-circuit line are independent, placed on the same towers or on two close towers for a portion of or the whole of their length. It can also occur if the circuits of the double-circuit line carry different amounts of active and reactive powers. Few related research works on this subject are available in the literature. To the knowledge of the authors, the effect on magnetic field and its polarization have not been fully covered in detail. Research works in [18, 19] showed that neglecting current phase shift effects in double-circuits led to significant errors in magnetic field calculations (larger than 45%) for human exposure [18] and between 10% and 75% for induced voltage on nearby buried metallic pipeline [19].

Although previous research works have established the effect of current phase shift and phase arrangements on the magnetic field distribution, this subject was not fully covered in the literature. The aim of this paper is to complete the previous mentioned works, by further establishing the effect of phase shift and phase arrangements using different power line configurations and giving a detailed analysis of the variation on the magnetic field distribution due to the effect of the current phase shifts. More so, the characteristics nature of the variations which was not considered in the previous research works [18, 19] is covered in this paper. In addition, the magnetic field polarization study and the pattern of its variations with current phase shifts and phase arrangements are also presented. The study is conducted for three phase balanced double-circuits transmission lines of vertical geometry in a Rand Water site in Gauteng Province, South Africa. The computation is done using analytical approach from field theory, for six phase arrangements with variations in current phase shift.

2. METHODS

2.1. Power Line Configurations and Network Model

The computation of the magnetic field distribution and polarization ratio due to double-circuits was performed for vertical configuration, based on the power line geometries sharing the same corridor with Rand Water pipelines at a location in Gauteng Province, South Africa. Figure 1(a) shows the geometrical configuration of the three-phase double-circuits vertical power line geometry with phase conductors labelled A, B, and C. The two circuits are separated by W, and H_t is the distance of the lowest conductor from the ground at the tower.

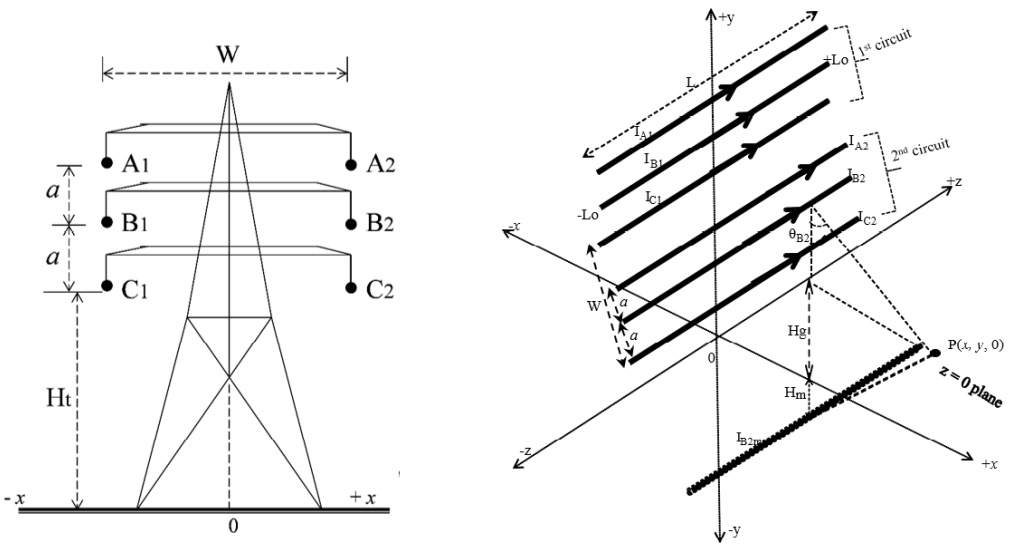

Figure 1. Schematic of the study power line network, (a) double-circuits vertical configuration, (b) the model for the field calculation due to the double-circuits line.

In Figure 1(b), the model for the field distribution and polarization calculation due to the double-circuits line is presented. Cartesian coordinate system is used. The vertical plane is chosen to lie on point $P(x, y, 0)$, i.e., $z = 0$ plane on which the point of observation lies. Height is represented with y-axis, and the clearance of the lowest conductor to the ground of mid-span between two towers is H_g. For easy analysis, the two parallel circuits are placed to be equidistant from the y-axis.

For the computations, some assumptions and simplifications are made. All conductors constituting the line are considered as infinitely long straight wires at constant height from the soil, horizontal, and parallel to each other. Although the effect of conductor sag is taken care of in the values of the ground clearance H_g, the medium is assumed to be linear, and the ground is assumed to be flat, free of irregularities, conductive but magnetically transparent and of homogenous resistivity. Typical values of the relative permeability of various soils and rocks range from 1.00001 to 1.136 except rocks in iron-mining areas [20]. The presence of towers, utility poles, buildings, vegetation and any other objects in the area is neglected. Since the power line frequency is 50 Hz, the magnetic field is treated as a quasi-static field [21–23]. The calculation of the magnetic field is reduced to a simple plane problem because the situation is exactly the same on every section of the line given the above assumptions and simplifications. Using the above assumptions, a two-dimensional analysis is sufficiently accurate using Biot-Savart law, image method and the superposition principle [21, 23]. The principle of superposition can be applied to the field values generated by all the straight line segments to provide the total field at a point of interest $P(x, y, 0)$ using the linearity properties of the surrounding medium (air-soil). Also, the Biot-Savart law is sufficient for computing the magnetic field contribution due to the eddy currents induced in metallic structures at the point $P(x, y, 0)$ adjacent to the power lines. Additionally, since the ground is considered to be conductive and magnetically transparent, the currents induced in the ground due to its finite resistivity can be accounted for through the image current approach [21, 23]. The quasi-static field of a magnetic line source in free space above the earth is equivalent to the magnetic field of the line source plus a complex image in free space. The image currents are negative with respect to the line currents [14].

If the line source is located at height y_i above the plane, the complex image is a line source at a complex depth equal to $y_i + \delta(1 - j)$ where

$$\delta = \sqrt{\frac{\rho}{\mu_o \pi f}}. \tag{1}$$

In Eq. (1), δ is the earth's skin depth (depth of penetration), ρ the resistivity of the earth, μ_o the

permeability of free space, and f the frequency of the source current. Typical values of earth resistivity range from 10 to 1000 Ωm; therefore, the image currents are located at hundreds of meters below the ground.

In Figure 1(b), considering the conductor with current I_{B2}, there is an image conductor at a depth H_m below the ground. If L is the length of the conductor, and L_o is half of the conductor length, then at a point $P(x, y)$ on the $z = 0$ plane, the horizontal component of the magnetic flux density due to the phase conductor with current I_{B2} is

$$B_{B2x} = -B_{gB2}\left(\frac{y_{B2} - y}{d_{B2}}\right) - B_{mB2}\left(\frac{y - y_{B2m}}{d_{B2m}}\right), \tag{2}$$

and the vertical component of the magnetic flux density due to the phase conductor is

$$B_{B2y} = -B_{gB2}\left(\frac{x - x_{B2}}{d_{B2}}\right) + B_{mB2}\left(\frac{x - x_{B2m}}{d_{B2m}}\right), \tag{3}$$

where

$$B_{gB2} = \frac{\mu_o I_{B2} L_o}{2\pi d_{B2}\sqrt{L_o^2 + d_{B2}^2}}, \tag{4}$$

$$B_{mB2} = \frac{\mu_o I_{B2} L_o}{2\pi d_{B2m}\sqrt{L_o^2 + d_{B2m}^2}}, \tag{5}$$

$$d_{B2} = \sqrt{(y_{B2} - y)^2 + (x - x_{B2})^2}, \tag{6}$$

and

$$d_{B2m} = \sqrt{(y - y_{B2m})^2 + (x - x_{B2m})^2}. \tag{7}$$

In real situations, the length of the phase conductors is much greater than the distance from point P; therefore, the calculation of the magnetic flux density can be performed directly from Ampere's theorem. Thus the relations in Eqs. (4) and (5) become simpler. In Figure 1(b), $y_{B2} = H_g + a$, $x_{B2} = x_{B2m} = W/2$, and $y_{B2m} = -(H_g + a + \delta)$. Similar expressions can be derived for the magnetic flux density due to all the other phase conductors in the two circuits.

Assuming the steady state current in the three-phase conductors of a circuit varies as $\sin \omega t$, with a phase angle φ to one another, then at point P, the total time-varying horizontal component and total time-varying vertical component of the magnetic flux density $B_{Rx}(t)$ and $B_{Ry}(t)$, respectively, are expressed as

$$\begin{aligned} B_{Rx}(t) &= k_1 \sin \omega t + k_2 \cos \omega t \\ B_{Ry}(t) &= k_3 \sin \omega t + k_4 \cos \omega t \end{aligned} \tag{8}$$

where for phase arrangement $\mathrm{A_1B_1C_1 - A_2B_2C_2}$ (untransposed phase arrangement), and phase currents of circuit 2 having a phase shift α to the corresponding phase currents of circuit 1,

$$\begin{aligned} k_1 = {} & B_{B1x} + B_{B2x}\cos\alpha + \cos\varphi\,(B_{A1x} + B_{A2x}\cos\alpha + B_{C1x} + B_{C2x}\cos\alpha) \\ & + \sin\alpha \sin\varphi\,(B_{C2x} - B_{A2x}) \\ k_2 = {} & \sin\varphi\,[(B_{A1x} + B_{A2x}\cos\alpha) - (B_{C1x} + B_{C2x}\cos\alpha)] + \sin\alpha\cos\varphi\,(B_{C2x} + B_{A2x}) \\ k_3 = {} & B_{B1y} + B_{B2y}\cos\alpha + \cos\varphi\,(B_{A1y} + B_{A2y}\cos\alpha + B_{C1y} + B_{C2y}\cos\alpha) \\ & + \sin\alpha \sin\varphi\,(B_{C2y} - B_{A2y}) \\ k_4 = {} & \sin\varphi\,[(B_{A1y} + B_{A2y}\cos\alpha) - (B_{C1y} + B_{C2y}\cos\alpha)] + \sin\alpha\cos\varphi\,(B_{C2y} + B_{A2y}) \end{aligned} \tag{9}$$

k_1 and k_3 are the in-phase components of the horizontal and vertical components of the magnetic flux density, respectively, and k_2 and k_4 are the out-of-phase components of the horizontal and vertical components of the magnetic flux density, respectively.

The magnitude of the total horizontal component and magnitude of the total vertical component respectively are

$$\begin{aligned} |B_{Rx}| &= \sqrt{k_1^2 + k_2^2} \\ |B_{Ry}| &= \sqrt{k_3^2 + k_4^2} \end{aligned} \tag{10}$$

The magnitude of the resultant magnetic flux density is

$$|B_R| = \sqrt{|B_{Rx}|^2 + |B_{Ry}|^2} \tag{11}$$

From IEEE Standard 644-19954 [24], the resultant field can also be expressed as;

$$|B_R| = \sqrt{B_{\max}^2 + B_{\min}^2} \tag{12}$$

where $B_{\max}$ and $B_{\min}$ are the values of the semi major and semi minor axes of the magnetic field ellipse, respectively. If the magnetic field is linearly polarized, $B_{\min} = 0$ and $B_R = B_{\max}$. If the magnetic field is circularly polarized, $B_{\max} = B_{\min}$ and $B_R = 1.41 B_{\max}$. If $B_{\min}$ is less than $B_{\max}$, the magnetic field is elliptically polarized.

The values of $B_{\min}$ and $B_{\max}$ can be obtained from k_1, k_2, k_3 and k_4 as shown in Eqs. (13)–(15).

$$B_{\min} = \min\left(B_R(t)\right)_{t:\,0-T}, \tag{13}$$

and

$$B_{\max} = \max\left(B_R(t)\right)_{t:\,0-T} \tag{14}$$

where

$$B_R(t) = \sqrt{\frac{k_1^2 + k_2^2 + k_3^2 + k_4^2}{2} + \left(\frac{k_2^2 + k_4^2 - k_1^2 - k_3^2}{2}\right)\cos 2\omega t + (k_1 k_2 + k_3 k_4)\sin 2\omega t} \tag{15}$$

with t ranging from 0 to T where T is the period of a cycle.

2.2. Parameters Used for Computation

For the power line at the site, symmetrical load current of 400 A and earth's resistivity of 100 Ωm are used for the computation. The two circuits are assumed to carry the same amount of load current, and effects of overhead earth wires on the circuits are neglected. As shown in Figure 1(a), a is 10 m, W 15 m and H_t 22 m. Given a maximum mid-span sag of 10 m, the mid-span ground clearance H_g is 12 m. In the computation, the planar magnetic flux density distributions below the power lines, as well as the polarization ratio, are obtained for a balanced system in which the currents in the conductors are at a phase angle φ of 120° to one another. The computation of the polarization ratio is obtained for points at 1 m by 1 m resolution, and the current phase shifts between the circuits is considered from −180° to +180°. Computations are performed for six possible different phase arrangements of the double-circuits, and the combinations are ABC-ABC, ABC-CBA, ABC-BAC, ABC-CAB, ABC-ACB and ABC-BCA. MATLAB software is used for the computation and result presentation.

3. RESULTS AND DISCUSSION

3.1. Magnetic Field Distribution Lateral Profiles

Figure 2 shows the lateral profile of the resultant magnetic flux density of all the six phase arrangements with a phase shift of 0° between the corresponding phase currents of the two circuits. For all the phase arrangements, the strength of the magnetic flux density decreases with distance. For lower ground clearance, the maximum value of the flux density for the transposed arrangement will be higher than the untransposed while at higher ground clearance, the reverse is the case.

Considering the symmetry of the lateral profiles, phase arrangements ABC-CAB and ABC-BCA show off-side asymmetry, while the rest are symmetrical about the centre of separation of the two

circuits. Therefore, the lateral distribution of the magnetic flux density below the power lines also depends on the phase arrangement of the conductors.

One observation in Figure 2 is that, outside the outermost conductors of the double-circuits, the field profiles of all the phase arrangements occupy different lateral widths at a field level of 1 μT. In this case, the untransposed phase arrangement ABC-ABC has the longest lateral width, and the directly transposed phase arrangement ABC-CBA has the shortest lateral width.

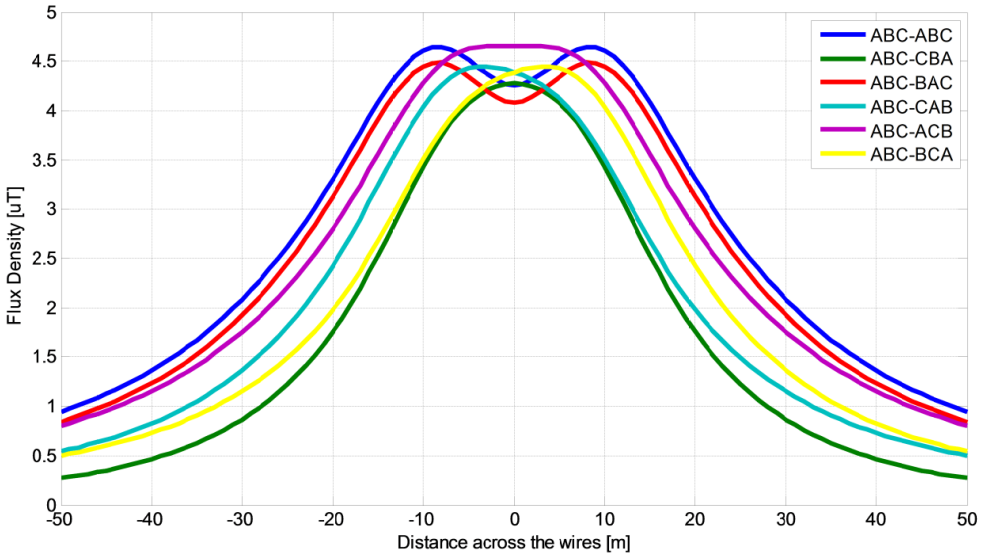

Figure 2. Lateral profile of the resultant magnetic flux density at ground level of all the six phase arrangements with a phase shift of 0° between the corresponding phase currents of the two circuits.

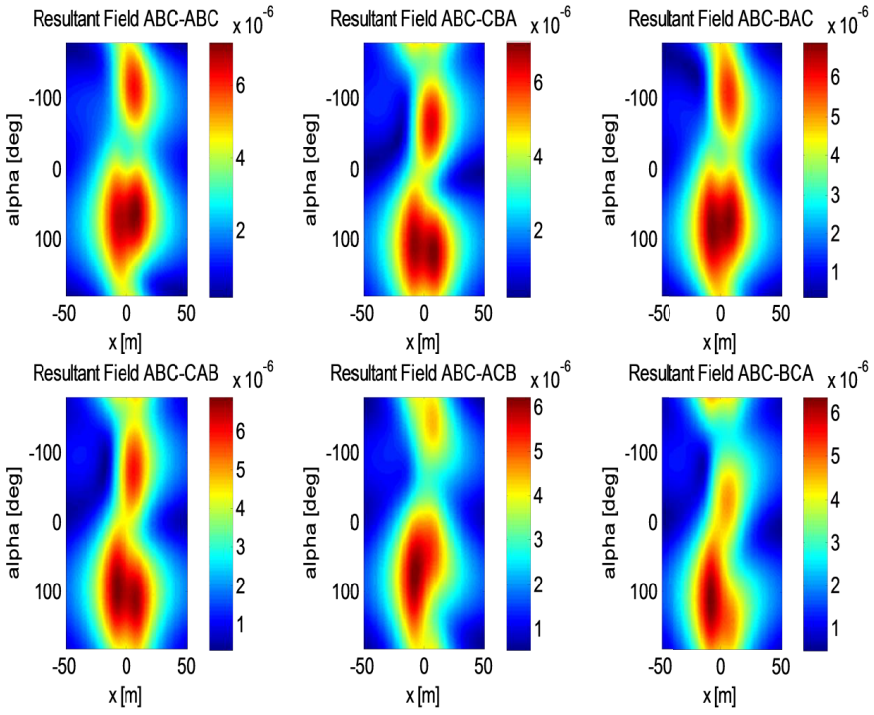

Figure 3. Lateral distribution at the ground level of the resultant magnetic flux density with variations in current phase shift, for all the six phase arrangements.

3.2. Lateral Profiles of the Resultant Field with Current Phase Shift

Figure 3 shows the lateral distribution at the ground level of the resultant magnetic flux density in the transverse plane across the axis of the conductors with variations in current phase shift from $-180°$ to $+180°$, for all the six phase arrangements.

Considering the distribution pattern, it can be observed that the lateral profiles and the intensity of the resultant field vary with the current phase shift angle α as revealed in [18]. Also, the largest and smallest widths of the field profiles for each phase arrangement occur at different angles of the current phase shift. The pattern of variation for each phase arrangement can be observed to be unique, even though some arrangements tend to show some similarity of patterns (e.g., pattern of variation for phase arrangements ABC-ABC/ABC-BAC, and ABC-CBA/ABC-CAB).

In Figure 3, the field lateral profile of some phase arrangements at a current phase shift of $0°$ is equivalent to the field lateral profile of some arrangements at $120°$ or $-120°$ though it may not be obvious in the figures. With these variations in the resultant field due to variations in the current phase shift (which could be time-dependent), there are also variations in the horizontal component of the magnetic field with current phase shift. Consequently, this brings about variation in the induced

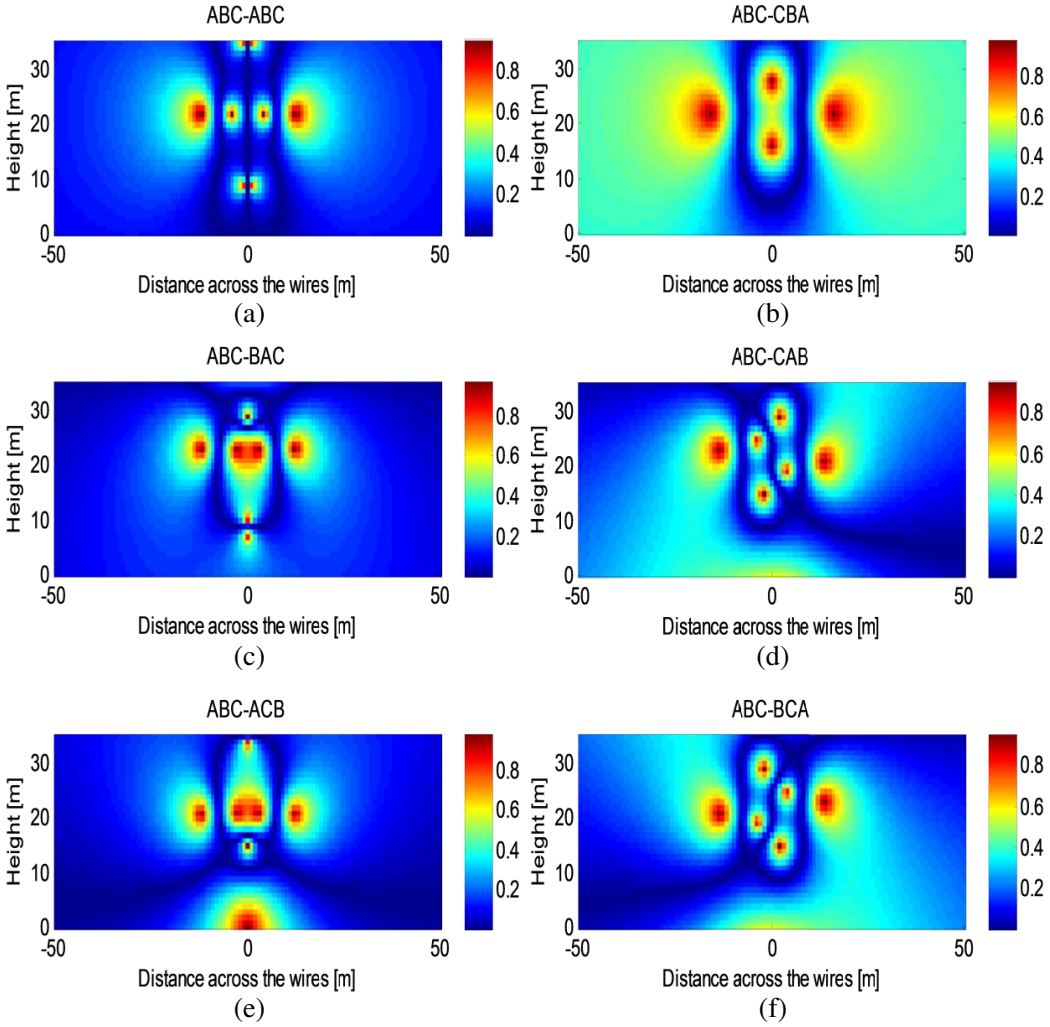

Figure 4. Spatial polarization ratio distribution of the magnetic flux density, of the balanced double-circuit, vertical configuration, of all the six phase arrangements with a phase shift of $0°$ between the corresponding phase currents of the two circuits.

voltage on buried metallic pipelines in the vicinity of the lines [19]. It should be noted that the patterns shown in Figure 3 are for balanced circuits with the same magnitude of current flowing in the two circuits. Different patterns will be observed for unbalanced conditions on the lines.

3.3. Field Polarization

Figure 4 shows the distribution of the polarization ratio of the magnetic flux density in the transverse plane around the balanced double-circuit, vertical geometry power line. This is considered for all the six phase arrangements with a phase shift of 0° between the corresponding phase currents of the two circuits. From Figure 4(a) it can be observed that, for the untransposed circuit ABC-ABC at the ground level, the polarization is linear within the separation of the two circuits. This can still be considered linear for far distances from the circuit. In Figure 4(b), for the directly transposed phase arrangement ABC-CBA, at the ground level, the polarization is elliptical throughout, though it tends to being linear within the separation of the two circuits. At distances greater than 35 m from the centre of separation of the two circuits at the ground level, phase arrangements ABC-BAC and ABC-ACB (Figure 4(c) & Figure 4(e) show linear polarization. However, ABC-ACB has a circular polarization at the mid-distance of separation of the two circuits.

The symmetrical patterns of the untransposed phase arrangement in Figure 4(a) and the directly transposed phase arrangement in Figure 5(b) are unique. The patterns of phase arrangements ABC-BAC/ABC-ACB (Figure 4(c) & Figure 4(e)) and ABC-CAB/ABC-BCA (Figure 4(d) & Figure 4(f)) exhibit mirror reflection symmetry of each other.

3.4. Polarization Ratio Profiles Due to the Current Phase Shifts

As the magnetic field distributions vary with variations in the phase shift of corresponding phase currents of the double-circuits, the field polarization shapes are also expected so. This is observed by considering

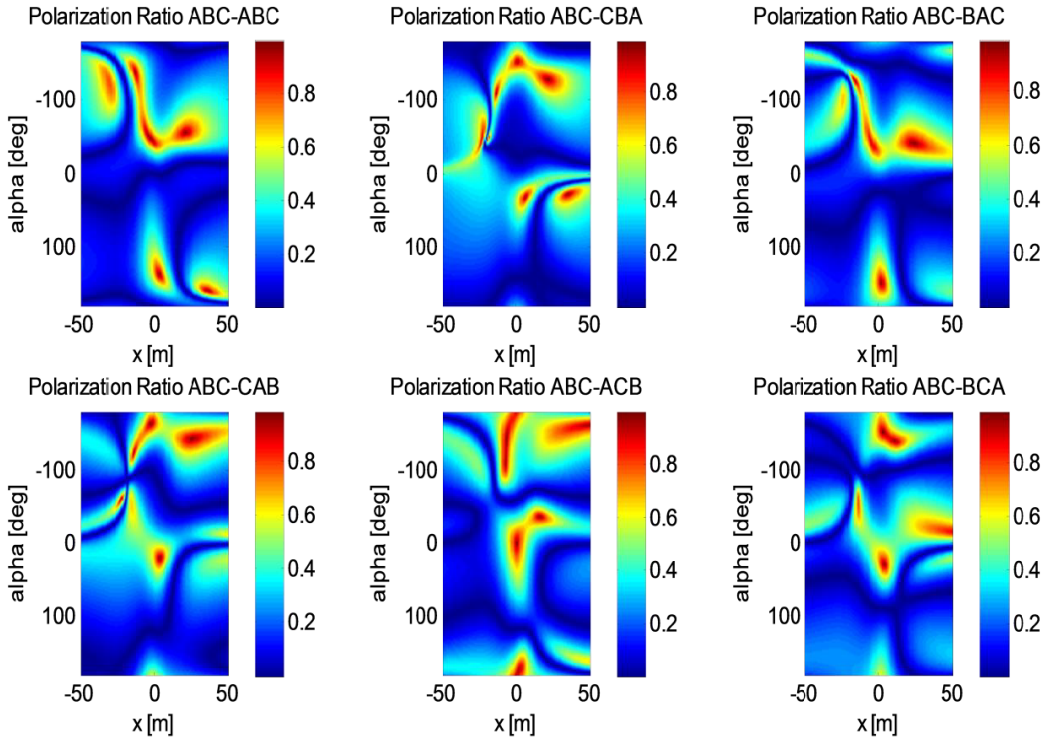

Figure 5. Lateral polarization ratio profile at the ground level of the magnetic flux density with variations in current phase shift, of the balanced double-circuit, vertical configuration, for all the six phase arrangements.

the polarization ratio at the ground level in the transverse plane. In Figure 5, the lateral profile of the polarization ratio of the magnetic flux density at the ground level in the transverse plane is presented. In this case, the variations in current phase shift from $-180°$ to $+180°$, of the balanced double-circuits, vertical and horizontal configurations for all the six phase arrangements are considered.

It can be observed that for the configuration of the double-circuits considered in this paper, the lateral profiles of the field polarization ratio vary with the current phase shift angle α, for all the six phase arrangements. The pattern of variation for each phase arrangement can be observed to be unique with no similarity of patterns, though the lateral profile of the polarization ratio of some phase arrangements at a current phase shift of $0°$ may be similar to the lateral profile of some arrangements at $120°$ or $-120°$.

4. CONCLUSION

The influence of the current phase shift and phase arrangement of multi-circuits power lines on the planar magnetic field distribution and its spatial polarization cannot be overlooked. The results presented reveal that the magnetic field strength at the ground level and the pattern of the field polarization below the conductors depend, among other factors, on the conductors' phase sequence arrangements and the phase shifts between the corresponding currents of the two circuits. Although this is in line with the findings in [18] and some other works in the literature, in the present study, not only the variation of the filed distribution with phase arrangements and phase shifts is further established, but also the characteristic nature of the variation of the field distribution for the six cases is examined in more detail. In addition, the study also examines the spatial polarization of the field and its pattern of variation with the current phase shift and phase arrangements. Information about the field component distribution and the spatial polarization pattern at ground level due to power lines is crucial because of its impact on aerial and buried conducting structures as well as on human bodies in its vicinity.

In placing metallic pipelines near AC multi-circuits HVTLs, it is essential to consider the field distribution by the phase arrangement of the line and the current phase shift by either computations or measurement and the pipelines placed in the region of minimum field intensity within the allowable servitude of the line.

Conflicts of Interest

The authors of this work declare no conflicts of interests.

ACKNOWLEDGMENT

This work was supported by Rand Water and the National Research Foundation of South Africa.

REFERENCES

1. Ahmed, H., M. Wael, and A. Ehab, "Effects of electromagnetic field from power line on metallic objects and human bodies," *International Journal of Electromagnetics and Applications*, Vol. 2, No. 6, 151–158, 2012.
2. Lopez, A. N., J. Gonzalez-Rubio, J. M. Montoya, and E. A. Garde, "Using multiple exposimeters to evaluate the influence of the body when measuring personal exposition to radio frequency electromagnetic fields," *COMPEL: The International Journal for Computation and Mathematics in Electrical and Electronic Engineering*, Vol. 34, No. 4, 1063–1069, 2015.
3. Christoforidis, G. C., D. P. Labridis, and P. S. Dokopoulos, "Inductive interference calculation on imperfect coated pipelines due to nearby faulted parallel transmission lines," *Electric Power Systems Research*, Vol. 66, No. 2, 139–148, 2003.
4. Christoforidis, G. C., D. P. Labridis, and P. S. Dokopoulos, "Inductive interference on pipelines buried in multilayer soil due to magnetic fields from nearby faulted power lines," *IEEE Transactions on Electromagnetic Compatibility*, Vol. 47, No. 2, 254–262, 2005.

5. Micu, D. D., L. Czumbil, G. C. Christoforidis, A. Ceclan, and D. Stet, "Evaluation of induced AC voltages in underground metallic pipeline," *COMPEL: The International Journal for Computation and Mathematics in Electrical and Electronic Engineering*, Vol. 31, No. 4, 1133–1143, 2012.
6. Adedeji, K. B., A. A. Ponnle, B. T. Abe, and A. A. Jimoh, "Analysis of the induced voltage on buried pipeline in the vicinity of high AC voltage overhead transmission lines," *Proceedings of the 23rd Southern African Universities Power Engineering Conference*, 7–12, Johannesburg, Jan. 28–30, 2015.
7. Ouadah, M., O. Touhami, and R. Ibtiouen, "Diagnosis of AC corrosion on the buried pipeline due to the high voltage power line," *Journal of Electrical Engineering*, Vol. 16, 76–83, 2016.
8. Ponnle, A. A., K. B. Adedeji, B. T. Abe, and A. A. Jimoh, "Variation in phase shift of multi-circuit HVTLs phase conductor arrangements on the induced voltage on buried pipeline: A theoretical study," *Progress In Electromagnetic Research B*, Vol. 69, 75–86, 2016.
9. Jiang, Z., Y. Du, M. Lu, Y. Zhang, D. Tang, and L. Dong, "New findings on the factors accelerating AC corrosion of buried pipelines," *Corrosion Science*, Vol. 81, 1–10, 2014.
10. M'hamed, O., Z. Mourad, Z. Aicha, T. Omar, I. Rachid, B. Saida, and D. Cherif, "AC corrosion induced by HVTL on cathodically protected pipelines," *Proceedings of International Conference on Control, Engineering and Information Technology (CEIT'14)*, 22–26, Sousse, Tunisia, Mar. 22–25, 2014.
11. Ouadah, M., O. Touhami, and R. Ibtiouen, "Diagnosis of the AC current densities effect on the cathodic protection performance of the steel x70 for a buried pipeline due to electromagnetic interference caused by HVPTL," *Progress In Electromagnetics Research M*, Vol. 45, 163–171, 2016.
12. Ponnle, A. A., K. B. Adedeji, B. T. Abe, and A. A. Jimoh, "Spatial magnetic field polarization below balanced double-circuit linear configured power lines for six phase arrangements," *Proceedings of the ACEMP-OPTIM-ELECTROMOTION Joint Conference*, 163–169, Side, Turkey, Sep. 2–4, 2015.
13. Mamishev, A. V. and B. D. Rusell, "Measurement of magnetic fields in the direct proximity of power line conductors," *IEEE Transactions on Power Delivery*, Vol. 10, No. 3, 1211–1216, 1995.
14. Milutinov, M., A. Juhas, and M. Prsa, "Electromagnetic field underneath overhead high voltage power line," *Proceedings of the 4th International Conference on Engineering Technologies*, Novi Sad, Apr. 28–30, 2009.
15. Mazzanti, G., M. Landini, and E. Kandia, "A simple innovative method to calculate the magnetic field generated by twisted three-phase power cables," *IEEE Transactions on Power Delivery*, Vol. 25, No. 4, 2646–2654, 2010.
16. Mazzanti, G., M. Landini, E. Kandia, and L. Sandrolini, "Simple calculation method of the magnetic field from double-circuit twisted three-phase cables as a tool for fault detection," *Proceedings of 8th IEEE Symposium on Diagnostics for Electrical Machines, Power Electronics and Drives*, Bologna, Sep. 5–8, 2011.
17. Mazzanti, G., M. Landini, E. Kandia, C. Biserni, and M. Marzinotto, "Innovative calculation methods of the magnetic field from single and double-circuit twisted three-phase cables widely used in MV and LV installations," *Central European Journal of Engineering*, Vol. 2, No. 2, 212–223, 2012.
18. Mazzanti, G., "Current phase-shift effects in the calculation of magnetic fields generated by double-circuit overhead transmission lines," *Proceedings of IEEE Power Engineering Society General Meeting*, 1–6, Denver, Jun. 6–10, 2004.
19. Micu, D. D., G. C. Christoforidis, and L. Czumbil, "AC interference on pipelines due to double-circuit power lines: A detailed study," *Electric Power Systems Research*, Vol. 103, 1–8, 2013.
20. Scott, J. H., "Electrical and magnetic properties of rock and soil," US Geological Survey Technical Letter, Special Projects-16, 1966.
21. Wait, J. R. and K. P. Spies, "On the image representation of the quasi-static fields of a line current," *Canadian Journal of Physics*, Vol. 47, 2731–2733, 1969.
22. Olsen, R. G. and P. S. Wong, "Characteristics of low frequency electric and magnetic fields in the vicinity of electric power lines," *IEEE Transactions on Power Delivery*, Vol. 7, 2046–2053, 1992.

23. Lindell, I. V., J. I. Hanninen, and R. Pirjola, "Wait's complex image principle generalized to arbitrary sources," *IEEE Transactions on Antennas and Propagation*, Vol. 48, 1618–1624, 2000.
24. IEEE Standard 644-19954, "Standard procedures for measurement of power frequency electric and magnetic fields from AC power lines," IEEE Standard 644–19954, 1–3, 1995.